Shock and Vibration 20 (2013) 809–819
DOI 10.3233/SAV-130786
IOS Press

An electrostatically actuated MEMS arch band-pass filter

Hassen M. Ouakad
Department of Mechanical Engineering, King Fahd University of Petroleum and Minerals 31261, Dhahran, Kingdom of Saudi Arabia
E-mail: houakad@kfupm.edu.sa

Received 11 September 2012
Revised 13 December 2012
Accepted 2 March 2013

Abstract. This work presents an investigation of the dynamics of micromachined arches resonators and their potential to be utilized as band-pass filters. The arches are actuated by a DC electrostatic load superimposed to an AC harmonic load. The dynamic response of the arch is studied analytically using a Galerkin-based reduced-order model when excited near its fundamental and third natural frequencies. Several simulation results are presented demonstrating interesting jumps and snap-through behavior of the arches and their attractive features for uses as band-pass filters, such as their sharp roll-off from pass bands to stop bands and their flat response.

Keywords: MEMS, arches, filters, dynamic snap-through

1. Introduction and background

1.1. Introduction

Thanks to the advances in research in the area of wireless communications, we have seen the development of the so-called microelectromechanical (MEMS) filters that have the advantages of being small, of low power consumption, of low cost, and of high quality factors. Add to that, the evolution of MEMS technology has led to a new generation of filters based on microbeams. Many groups [1–11] presented several efficient ways to build such kind of filters, particularly band-pass filters, by simply exciting them near their resonant frequency (primary resonance excitation). This method has many advantages such as having a reasonable bandwidth. However, using merely the primary resonance does not prevent the structure from having measurable, and may be considerable, response outside the filtered region. In 1965, Nathanson et al. [1] discussed in details the design process of mechanical filters based on gold cantilever beams. Lin et al. [2] described a mechanical filter based on polysilicon interdigitated comb drive resonators with a double-folded support structure. Bannon et al. [3] presented the so-called H-shape filter, which is composed of two microbeams coupled by a weak microbeam. In another work [4], they described the design process of the H-shape filter and they reported a high quality filter when excited in the neighborhood of the center frequency (primary resonance). On other hand, many groups [5–11] tried to find well established techniques to enhance and optimize their filters specifications. Li et al. [5] achieved better results compared to [4] by using high-order modes to excite the filters and obtaining higher quality factor band-pass filters. Shaw et al. [6] analyzed the dynamics of MEMS oscillators based on parametric resonance and explored utilizing them as radio frequency filters. Their design is appropriate for highly tunable microbeams, which offer low-power consumption, and relatively simple integration with electronics. Rhoads et al. [7] described a filter design based on the nonlinear response of parametrically-excited MEMS oscillators. They showed desirable filtering features, such as an ideal stopband

ISSN 1070-9622/13/$27.50

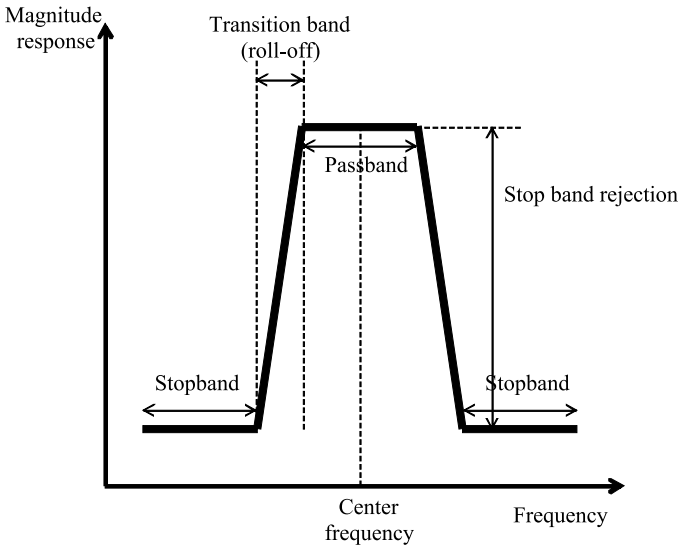

Fig. 1. Band-pass filter characteristics.

rejection behavior and a sharp response roll-off. Filter based on internal resonances were proposed by Vyas and Co-workers [8]. They [8] proposed a MEMS T-beam structure excited near its second resonance based on internal resonance. They obtained a non-zero output current for a band of frequencies by energy transfer from the second mode to the first mode. Hammad et al. [9,10] proposed to excite the H-shape filter fabricated by [4] at the sub-harmonic resonance of order one-half. They found that there are two bands where the trivial solution is unstable. These two bands correspond to the natural frequencies of the structure [10]. They also noted that the realization of single-valued responses for subharmonic excitation is not achievable for this H-shape band-pass filter. Greywall and Busch [11] demonstrated a new class of MEMS filters based on electrostatically-actuated drumhead resonators. The proposed filter was elastically coupled to produce a desirable band-pass frequency response.

Motivated by the need to further advance band-pass filters, we investigate the use of electrostatically actuated clamped-clamped arches as filters by exciting them by a DC and an AC harmonic load. Shallow arches have been under increasing focus in recent years in the MEMS community. A shallow arch is a beam, which is designed and fabricated to be curved without the need for an axial stress or buckling to form its shape. This kind of structure posses a bi-stable behavior, which has drawn attention for MEMS applications, especially as MEMS switches and actuators [12–19]. Recent works using static and transient models [18,19] have shown that initially curved clamped-clamped beams can undergo several scenarios of escapes via snap-through and pull-in instabilities due to DC electrostatic load.

In this paper, we study the possibility of building a filter based on the clamped-clamped MEMS arch by exciting it near one of its natural frequencies. Here, we will show examples of exciting the shallow arch near its first and third natural frequencies by a combined DC load and AC harmonic load.

1.2. Band-pass filter specifications

A band-pass filter is a system (mechanical, electrical, etc...) that allows signals to pass between two specific frequencies and filters the signals outside them. Band-pass filters are used primarily in wireless transmitters and receivers.

To illustrate the specification of a band-pass filter, we refer to the schematic shown in Fig. 1 for a filtered signal.

The most important characteristics of a band-pass filter shown in Fig. 1 are [3,4]:

- The center frequency, which is the nominal operating frequency of the filter.
- The band-pass, which is the range of frequencies in which the filter structure has the maximum energy and in which the signal is not filtered.

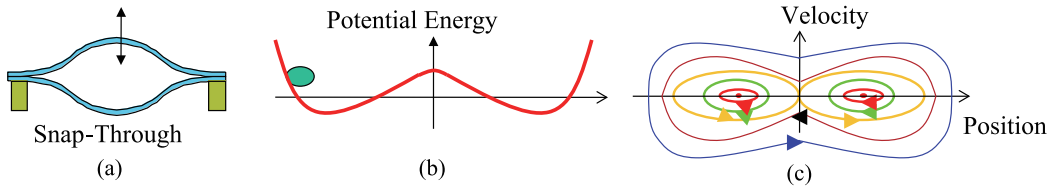

Fig. 2. (a) A shallow arch undergoing snap-through motion, (b) the total potential energy of the arch, (c) the corresponding phase portrait.

- The stopband rejection, which is the amount by which the signal is attenuated outside of the band-pass region.
- The transition band (roll-off), which is a measure of the transition from the band-pass region to the stopband one.

Note that ideal filters allow a specified range of frequency to pass through while attenuating a specified unwanted frequency range. Thus, a filter with ideal specifications would have a flat pass-band, completely filtered signals in the stopbands, and has instantaneous transition from the pass-band to the stop-band (sharp roll-off). Another important factor that measures the filter performance is its quality factor, which is directly related to the center frequency and the passband of the filter. In fact, it is high for high center frequency and narrow band-pass. This explains why MEMS groups have explored the use of clamped-clamped beam resonators rather than any other structures since they have typically high natural frequencies. In this paper, we explore clamped-clamped shallow arches, which have high natural frequencies.

1.3. Bistable behavior of a shallow arch

A shallow arch can vibrate either around its original deformed shape, around its opposing symmetric configuration, or can vibrate in between those two shapes (snap-through motion) with large amplitude of vibrations, Fig. 2(a). The potential energy of a shallow arch is of a double-well type, Fig. 2(b). With sufficient kinetic energy, a local vibration near one well can transfer to the other or escape to the global attractor in the case of snap-through motion, Fig. 2(c). The initial deformed configuration of the arch and its immovable edges results in strong influence of quadratic and cubic geometric nonlinearities on the structure behavior [20]. Because of its rich nonlinear phenomena, shallow arches and the problem of two-well potential have received special attention in the nonlinear dynamics literature [21].

The snap-through motion can be of static or dynamic nature [18,19,22]. Many previous investigations [23–25] addressed the possibility of triggering the pull-in instability by means of dynamic loading (either by transient effects [23,24] or by resonant external forces [25]). This is called “dynamic pull-in”, which characterizes the instability of the structure due to dynamics considerations. Snap-through of arches during their transient motion under uniform dynamic pressure loading has been reported in [26]. The fact that snap-through motion can be triggered by means of dynamic loading allows us to define “dynamic snap-through” which means snap-through due to dynamic effects.

1.4. Paper objective and organization

The objective of this paper is to study the dynamic behavior of an electrically actuated shallow arch and study the possibility of using its dynamics to build a simple band-pass filter.

The organization of this paper is as follows. In Section 2, we present a model for an electrically actuated clamped-clamped shallow arch. Section 3 summarizes the reduced-order model used in the simulations. In Section 4, we solve the static problem of the arch under the effect of DC electrostatic forces in order to ascertain the convergence of the reduced-order model. Section 5 presents the dynamics of the shallow arch when excited by a DC load superimposed to a small AC harmonic load near its first and third natural frequencies. Possibility of triggering the dynamic snap-through motion of the shallow arch and the utilization of this to realize new band-pass filters is investigated. Finally, we summarize the paper in the last section.

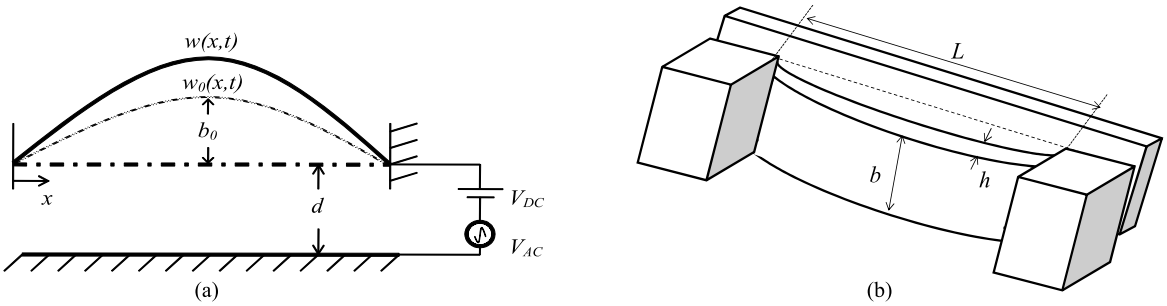

Fig. 3. (a) Schematic of the electrically actuated clamped-clamped arch, (b) a 3-D schematic picture of the arch.

2. Problem formulation

In this section, we formulate the problem governing the behavior of a MEMS shallow arch. Here, we consider a clamped-clamped shallow arch, Fig. 3, of initial shape $\hat{w}_0(\hat{x}) = b_o[1-\cos(2\pi x)]/2$, where b_0 is the initial rise, actuated by an electrode underneath it with a gap width d using a DC load superimposed to an AC harmonic load. Assuming Euler-Bernoulli beam model, the nonlinear equation of motion governing the transverse deflection $\hat{w}(\hat{x},\hat{t})$ of the arch of width b, thickness h, and length L is expressed as [18,20]

$$\begin{aligned} EI\frac{\partial^4\hat{w}}{\partial\hat{x}^4}+\rho A\frac{\partial^2\hat{w}}{\partial\hat{t}^2}+\tilde{c}\frac{\partial\hat{w}}{\partial\hat{t}} &= \frac{\varepsilon b[V_{DC}+V_{AC}\cos(\tilde{\Omega}\hat{t})]^2}{2(d-\hat{w}_0-\hat{w})^2} \\ &+\frac{EA}{2L}\left[\frac{\partial^2\hat{w}}{\partial\hat{x}^2}-\frac{\partial^2\hat{w}_0}{\partial\hat{x}^2}\right]\left[\int_0^L\left\{\left(\frac{\partial\hat{w}}{\partial\hat{x}}\right)^2-2\left(\frac{\partial\hat{w}}{\partial\hat{x}}\frac{\partial\hat{w}_0}{\partial\hat{x}}\right)\right\}d\hat{x}\right] \end{aligned} \tag{1}$$

where $E = 166$ GPa is the effective Young's modulus of the considered MEMS arch made of silicon, $A = bh$ is the cross-sectional area, $I = bh^3/12$ is the moment of inertia, $\rho = 2332$ kg/m^3 is the material density, $\varepsilon = 8.854\times 10^{-12}$ F.m^{-1} is the dielectric constant of the air, and $\tilde{c}$ is the viscous damping coefficient (here assumed to be linear since the gap width is large, which reduces any squeeze-film damping effect, and small since the arch is considered to operate at low pressure (under vacuum)).

The boundary conditions for a clamped-clamped arch beam are:

$$\hat{w}\left(0,\hat{t}\right)=0,\quad \frac{\partial\hat{w}}{\partial\hat{x}}\left(0,\hat{t}\right)=0,\quad \hat{w}\left(L,\hat{t}\right)=0,\quad \frac{\partial\hat{w}}{\partial\hat{x}}\left(L,\hat{t}\right)=0, \tag{2}$$

For convenience, we introduce the following nondimensional variables:

$$w=\frac{\hat{w}}{d},\quad w_0=\frac{\hat{w}_0}{d},\quad x=\frac{\hat{x}}{L},\quad t=\frac{\hat{t}}{T} \tag{3}$$

where T is a time constant defined by $T=\sqrt{\rho AL^4/EI}$. Next, we drop the hats for convenience.

Therefore, the nondimensional equations of motion and associated boundary conditions can be written as

$$\begin{aligned} \frac{\partial^4 w}{\partial x^4}+\frac{\partial^2 w}{\partial t^2}+c\frac{\partial w}{\partial t} &= \alpha_2\frac{[V_{DC}+V_{AC}\cos(\Omega t)]^2}{(1-w_0-w)^2} \\ &+\alpha_1\left[\frac{\partial^2 w}{\partial x^2}-\frac{\partial^2 w_0}{\partial x^2}\right]\left[\int_0^1\left\{\left(\frac{\partial w}{\partial x}\right)^2-2\left(\frac{\partial w}{\partial x}\frac{\partial w_0}{\partial x}\right)\right\}dx\right] \end{aligned} \tag{4}$$

$$w\left(0,t\right)=0,\quad \frac{\partial w}{\partial x}\left(0,t\right)=0,\quad w\left(1,t\right)=0,\quad \frac{\partial w}{\partial x}\left(1,t\right)=0, \tag{5}$$

where

$$\alpha_1=6\left(\frac{d}{h}\right)^2,\quad \alpha_2=\frac{\varepsilon bL^4}{2EId^3},\quad \Omega=\frac{\tilde{\Omega}}{\omega_n},\quad c=\frac{\tilde{c}L^4}{EIT}, \tag{6}$$

and $\omega_n=(4.73)^2\sqrt{EI/\rho AL^4}$.

3. The reduced-order model

To simulate response of the shallow arch, Eqs (4) and (5) are discretized using the Galerkin procedure to yield a Reduced-Order Model (ROM) [27,28]. The deflection of the shallow arch is approximated as

$$w(x,t) = \sum_{i=1}^{n} u_i(t)\phi_i(x), \tag{7}$$

where $\phi_i(x)$ $(i = 1, 2, \ldots, n)$ are the normalized linear undamped mode shapes of an unactuated straight microbeam, and $u_i(t)$ $(i = 1, 2, \ldots, n)$ are the nondimensional modal coordinates.

We will investigate the static as well as the dynamic behavior of the MEMS arch using the mode shapes of a straight beam, Eq. (8). This choice was based on many reasons: A comparison done in [29] in which we concluded that both approaches using either straight mode shapes or curved mode shapes in the ROM are showing acceptable agreement. The conclusion here is that using the mode shapes of a straight beam is sufficient to yield accurate results for arches and this confirms the approach used in [18] to study the static behavior of MEMS arches under electrostatic loads. Finally, from a computational point of view, straight-beam mode shapes are much favorable. Therefore, in this paper, we will use only the mode shapes of a straight beam as basis functions.

The mode shapes of the clamped-clamped straight beam are expressed as

$$\phi_i(x) = \cosh\beta_i x - \cos\beta_i x + \lambda_i\left(\sin\beta_i x - \sinh\beta_i x\right), \tag{8}$$

where: $\beta_i = \frac{(2i+1)\pi}{2}$, and $\lambda_1 = 0.9825$, $\lambda_i \approx 1$ for $i > 1$.

To obtain the ROM, we first multiply Eq. (4) by $F(x,t) = (1 - w_0 - w)^2$. Substituting Eq. (7) into the resulting equation, multiplying by $\phi_j(x)$, using the orthogonality conditions of the mode shapes, and then integrating the outcome from 0 to 1, we get differential equations in terms of the modal coordinates $u_i(t)$ given as follows

$$\begin{aligned}
&\sum_{i=1}^{n} \ddot{u}_i(t) \int_0^1 \{\phi_i(x)\phi_j(x)F(x,t)dx\} + c\sum_{i=1}^{n} \dot{u}_i(t) \int_0^1 \{\phi_i(x)\phi_j(x)F(x,t)\,dx\} \\
&\quad + \sum_{i=1}^{n} u_i(t) \int_0^1 \left\{\phi_i^{iv}(x)\phi_j(x)F(x,t)dx\right\} = \alpha_2[V_{DC} + V_{AC}\cos(\Omega t)]^2 \int_0^1 \phi_j(x)dx \\
&\quad + \alpha_1 \int_0^1 \left(\sum_{i=1}^{n} u_i(t)\phi_i'(x)\right)^2 dx \int_0^1 \{\phi_j(x)F(x,t)G(x,t)\}dx \\
&\quad - 2\alpha_1 \int_0^1 \left(\sum_{i=1}^{n} u_i(t)\phi_i'(x)\frac{\partial w_0}{\partial x}\right) dx \int_0^1 \{\phi_j(x)F(x,t)\,G(x,t)\}dx, \quad j = 1\ldots n
\end{aligned} \tag{9}$$

where

$$G(x,t) = \sum_{i=1}^{n} u_i(t)\phi_i''(x) - \frac{\partial^2 w_0}{\partial x^2}, \tag{10}$$

To simulate the dynamic behavior, those differential equations can be integrated with time. To simulate the static response, all time dependent terms in the differential equations are set equal to zero, then the modal coordinates $u_i(t)$ are replaced by unknown constant coefficients $a_i (i = 1, 2, \ldots, n)$. This results in a system of nonlinear algebraic equations in terms of the coefficients a_i. The system is then solved numerically using the Newton-Raphson method to obtain a_i and hence the static deflection of the arch.

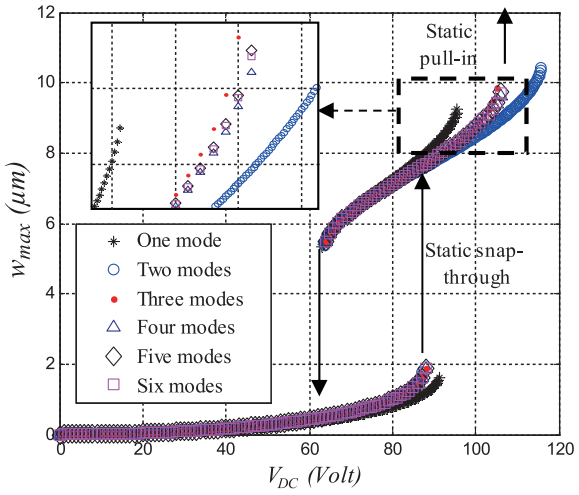

Fig. 4. Variation of the static deflection of the shallow arch with the DC voltage for various number of mode shapes of a straight beam in the ROM.

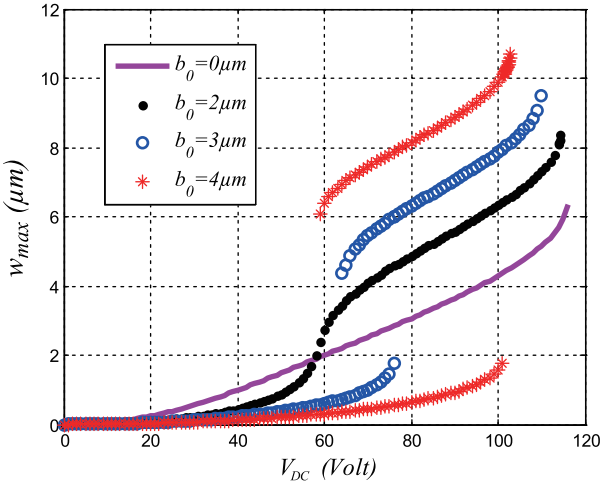

Fig. 5. Variation of the static deflection of the shallow arch with the DC voltage for various values of initial rise b_0.

4. The static response

In this section and as a case study, we consider the fabricated clamped-clamped shallow arch made of silicon of Krylov et al. [18] of $L = 1000$ μm, $h = 2.4$ μm, $b = 30$ μm, $d = 10.1$ μm, and initial rise $b_o = 3.5$ μm. Figure 4 shows the maximum static deflection of the shallow arch ($w_{\max} = w(x = 0.5)$) when using one up to six symmetric mode shapes of a straight clamped-clamped beam in the ROM while varying the DC load. It follows from the figure that using five symmetric modes yields acceptable converged results. As seen in the figure, the shallow arch undergoes a snap-through motion near $V_{DC} = 88$ V and then a pull-in instability near $V_{DC} = 106$ V. In all the next figures, we will be using five modes in the ROM.

In Fig. 5, the effect of the initial rise on the static deflection of the arch is shown. For the cases of $b_o = 3$ μm and $b_o = 4$ μm, the arch snaps-through first and pulls-in while increasing V_{DC}. However, for $b_o = 4$ μm the arch undergoes immediate pull-in after snap-through. The figure shows that the snap-through voltage increases and the pull-in voltage decreases when increasing the initial rise value of the shallow arch. This indicates that the stiffness of the shallow arch increases before snap-through and then decreases in the buckled position with the increase of b_o.

5. The dynamic response

Here, we study the dynamic behavior of the shallow arch due to a combined DC and AC harmonic loads. We integrate the differential equations, Eq. (9), in terms of the modal coordinates numerically with time using Runge-Kutta technique to simulate the dynamic response.

In Fig. 6, we simulate the dynamic response of the arch investigated in Section 4 with an initial rise of $b_o = 3$ μm to small values of DC and AC loads compared to the static pull-in value ($V_{DC} = 106$ V). Here, a damping ratio $\zeta = 0.1$ is assumed, which is related to the viscous damping coefficient c as $c = 2\zeta\omega$, where ω is the nondimensional fundamental natural frequency of an unactuated straight clamped-clamped beam. The figure shows primary and superharmonic resonances of order two, all of which are of softening-type behavior.

Next, we show in Fig. 7 the effect of the initial rise on the dynamic response of the arch. Results are also shown for $b_o = 0$ μm, which is the case of a straight clamped-clamped microbeam to enable comparison with arches . Note here that all the frequency-response curves start at $w_{\max} = w(x = 0.5)w_{\max}$ corresponding to the equilibrium position at $V_{DC} = 60$ V shown in Fig. 4 (quasi-static behavior at slow excitation frequency). First, one can see that there is an increase in the linear natural frequency of the arch with increasing b_o, as expected based on the conclusion that increasing b_o strengthens the stiffness of the arch, with the exception of the case of $b_o = 2$ μm. This

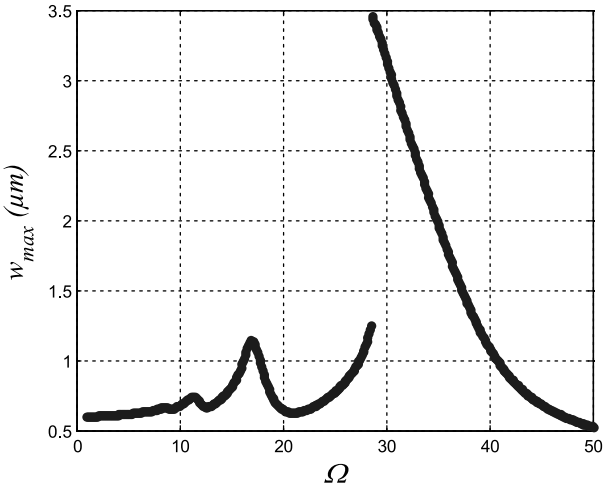

Fig. 6. Simulated frequency-response curve of a shallow arch actuated by DC and AC harmonic load for $b_0 = 3$ μm, $V_{DC} = 40$ V, and $V_{AC} = 20$ V.

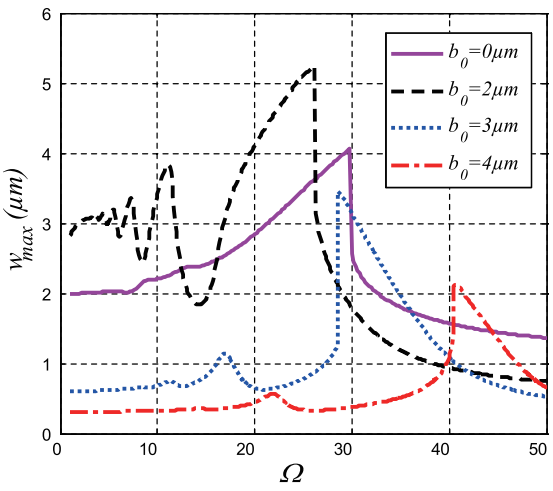

Fig. 7. Simulated frequency-response curves of a shallow arch actuated by DC and AC harmonic load for $V_{DC} = 40$ V, $V_{AC} = 20$ V, $\xi = 0.1$, and for various values of initial rise b_0.

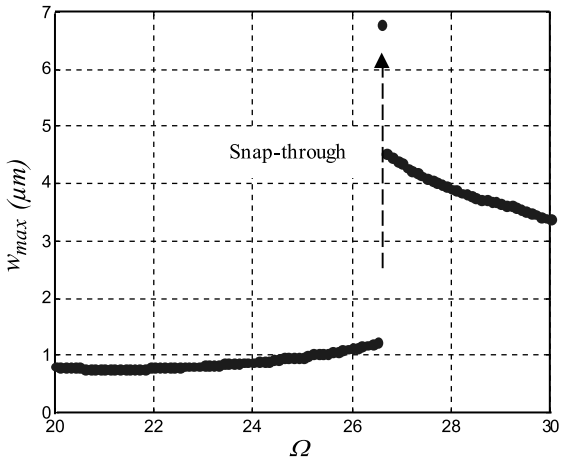

(a) V_{DC} =40 V, and V_{AC}=25 V

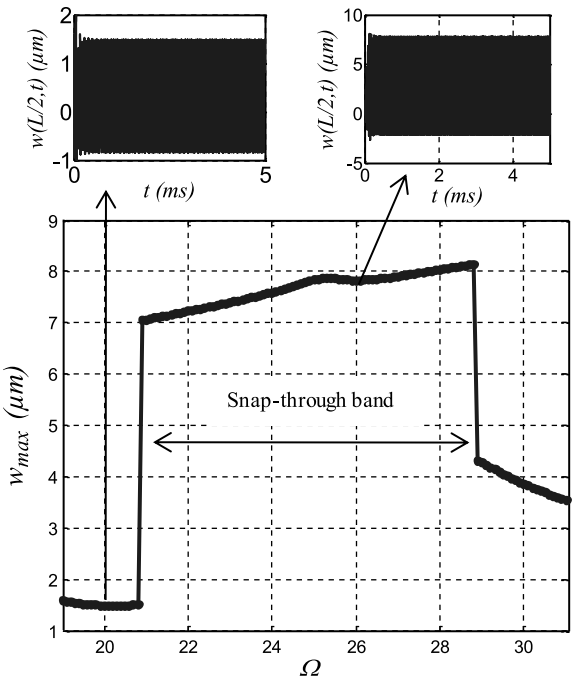

(b) V_{DC} =40 V, and V_{AC}=40 V

Fig. 8. Frequency-response curves of a shallow arch for an initial rise $b_0 = 3$ μm, damping ratio $\zeta = 0.1$, and for various AC loads.

is because at $V_{DC} = 60$ V, the curved beam in this case shows snap-through-like behavior, as seen in Fig. 5. For $b_o = 3$ μm and $b_o = 4$ μm, the frequency-response curve shows softening-type behavior. This indicates that the softening effects and the quadratic nonlinearities of the electrostatic force and the curvature are dominant. The cases of the straight microbeam and the "almost-curved" beam, $b_o = 2$ μm, show a hardening-type behavior. In this case the cubic mid-plane stretching effect dominates the other quadratic nonlinearities.

In the following, we focus on the snap-through phenomenon near primary resonance (excitation near the fundamental natural frequency). Consider the case of $b_0 = 3$ μm, $V_{DC} = 40$ V, and $\zeta = 0.1$. It turns out according to our

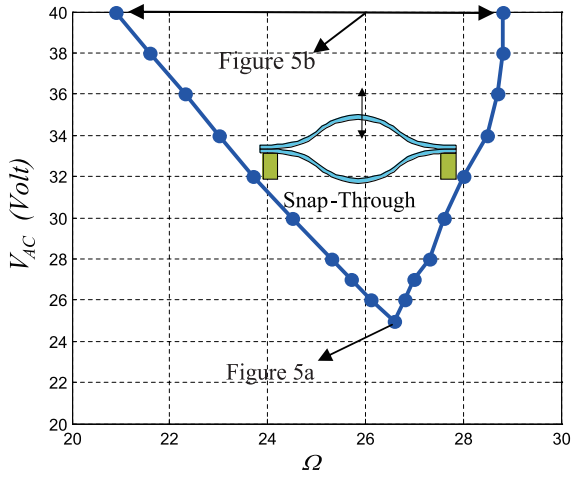

Fig. 9. The calculated snap-through band for $b_0 = 3$ μm, $V_{DC} = 40$ V, and $\zeta = 0.1$.

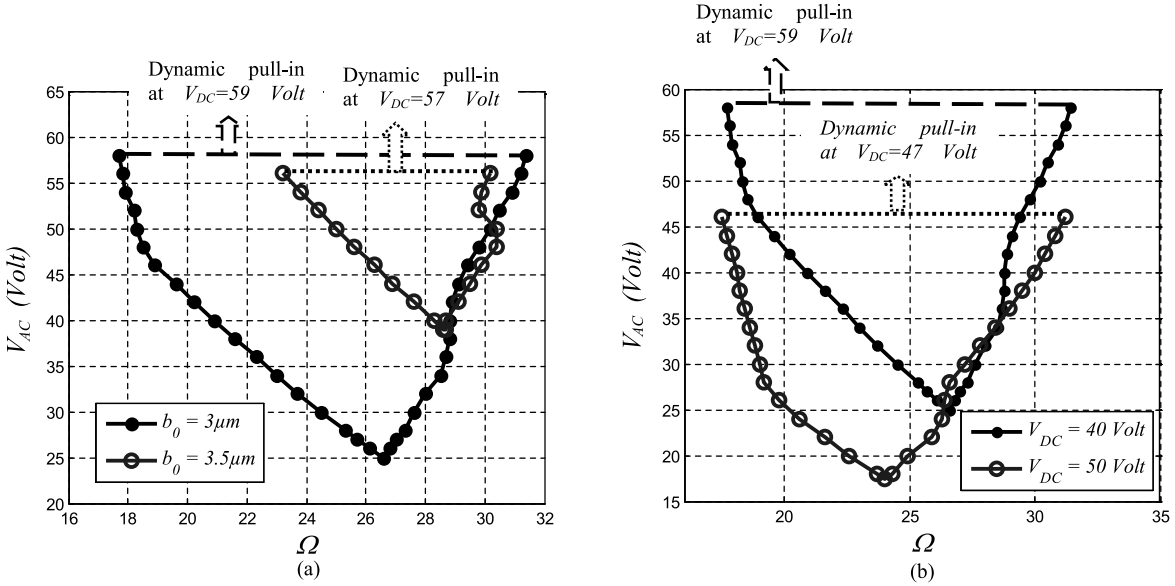

Fig. 10. The calculated snap-through bands (a) for $V_{DC} = 40$ V, $\zeta = 0.1$, and for different values of initial rise b_0, and (b) for $b_0 = 3$ μm, $\zeta = 0.1$, and two different DC voltages.

simulations that the arch starts to snap-through near its fundamental natural frequency at an AC load of $V_{AC} = 25$ V or higher, Fig. 5(a). Increasing V_{AC} beyond this value creates a frequency band where the arch is forced to snap-through if it is operated within this band. Figure 8(b) shows an example for the case of $V_{AC} = 40$ V. In this figure, if the arch is operated between $\Omega = 21$ and $\Omega = 28.5$, it vibrates in snap-through motion, i.e., in large motion compared to the vibration outside this band. This is further clarified in the insets of Fig. 8(b). This observation, in addition to the sharp jump in the response of the arch, opens the possibility of using this dynamical response of the arch as a band-pass filter. One can see from Fig. 8(b) that such a filter is characterized by a sharp transition from the pass-band $(21 < \Omega < 28.5)$ to the stop band and a flat bandwidth [30]. In addition, the bandwidth can be tuned through controlling the geometry of the device, such as the initial rise of the arch, the damping, and the electric loading. As an example, Fig. 9 shows the variation of the bandwidth for various values of V_{AC}. It is worth to mention here the shapes of the simulated snap-through bands are similar to the previously reported and measured pull-in bands in electrically actuated resonators [25].

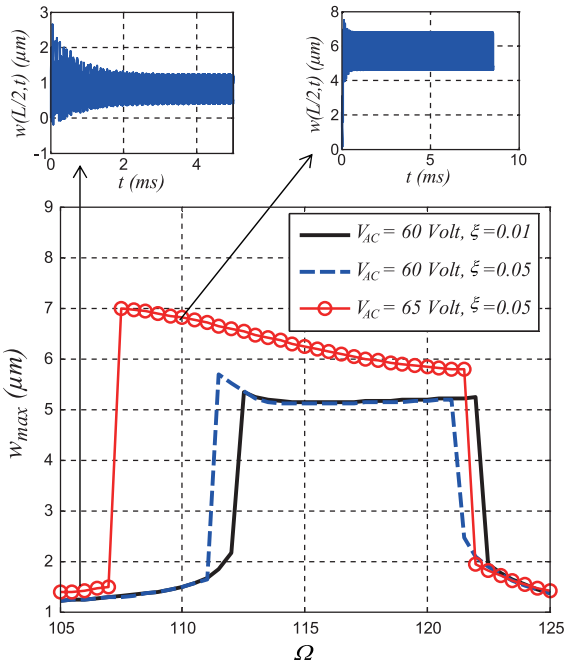

Fig. 11. Frequency-response curves of a shallow arch excited near its third mode for $b_0 = 3.5$ μm, $V_{DC} = 60$ V.

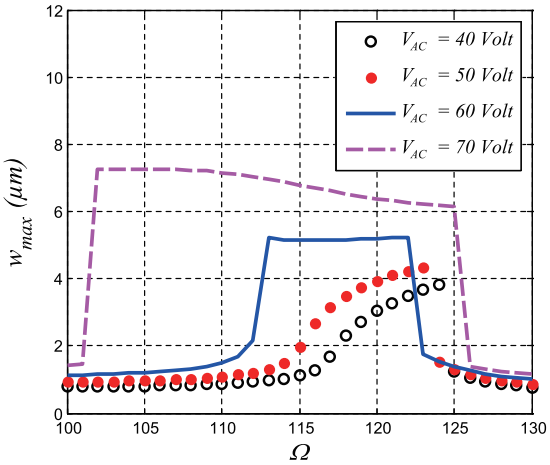

Fig. 12. Frequency-response curves of a shallow arch excited near its third mode for $V_{DC} = 60$ V.

In addition, the snap-through band can be tuned through controlling the geometry of the device, such as the initial rise of the arch, and the DC load. As an example, Figs 10(a) and (b) show the variation of the snap-through band for various values of V_{AC}, V_{DC}, and initial rise b_0. It should be mentioned that there is a limit of how much one can increase V_{AC} before reaching dynamic pull-in [25]. In the figures, we used bold arrows to indicate those dynamic pull-in values. We can also notice that if we increase the arch initial rise or the DC load, we decrease the value of the AC needed to get the pull-in limit. Also, increasing the initial rise shrinks the size of the obtained snap-through band, as noted from Fig. 10(a). It is worth to mention here that we did not talk much about what is happening near the superharmonic resonance of the arch and how this can affect the snap-through band near the primary resonance. This represents one limitation of our work that will be treated in a future investigation.

Next, we investigate the response of the arch when excited near its third natural frequency, Fig. 11. The figure indicates that the arch oscillates in small amplitude around one of its stable state before passing resonance. Then it jumps to the other symmetric well to vibrate in small motion around the other stable state for a wide range of frequencies, after which it returns back and jumps to its original potential well. This sort of result could be also promising to build a band-pass filter with a sharp roll off from the stop-band to pass-band, a flat bandwidth, and a high center frequency [30]. This kind of filter is very simple, easy to fabricate, and small in size compared to other MEMS filters, which are based on mechanically coupling two or more vibrating microstructures, which usually suffer mistuning problems and challenges in fabrication [30]. The same figure shows also that V_{AC} and the damping ratio can be used to control the bandwidth and the center frequency of such a filter.

Another major point that could be raised here that dynamic behavior of the arch near its third natural frequency is of hardening type and switch to the softening one after snap-through, Fig. 12 This behavior is totally the opposite of what we got when exciting the arch near its first natural frequency, Fig. 8.

6. Conclusion

In this paper, the potential to use the interesting dynamic behavior of an electrically actuated clamped-clamped shallow arch to realize band-pass filters is presented. Simulation results were shown demonstrating various scenarios

of dynamic snap-through motion near the first and the third natural frequencies. Promising results were shown for the possibility of using the dynamic snap-through motion of the arch near specific bands of frequencies to realize band-pass filters of sharp transition from the pass-band to stop-band and also of flat bandwidth. Also, a band-pass filter of higher center frequency was demonstrated by exciting the arch near its third mode.

Acknowledgment

The author is thankful to Professor M.I. Younis from the Department of Mechanical Engineering at SUNY Binghamton for introducing him to this world of MEMS arches.

References

[1] H.C. Nathanson and R.A. Wickstrom, A resonant gate silicon surface transistor with high Q bandpass properties, *IEEE Appl Phys Lett* **7** (1965), 84–86.
[2] L. Lin, C.T.C. Nguyen, R.T. Howe and A.P. Pisano, Micro electromechanical filters for signal processing, in: *Proc Workshop on Micro Electro Mechanical Systems*, Germany (1992), 226–231.
[3] F.D. Bannon, J.R. Clark and C.T.C. Nguyen, High frequency microelectromechanical IF filter, in: *Proc Int Electon Devices Meeting* (1996), 773–779.
[4] F.D. Bannon, J.R. Clark and C.T.C. Nguyen, High-Q HF microelectromechanical filters, *J Solid-State Circuits* **35** (2000), 512–526.
[5] S.S. Li, M.U. Demirci, Y.W. Lin, Z. Ren and C.T.C. Nguyen, Bridged micromechanical filters, in: *Proc IEEE Int Ultrasonics, Ferroelectrics and Frequency Control Joint 50 Anniversary Conference*, Montreal, Canada (24–27 Aug 2004), 280–286.
[6] S. Shaw, K. Turner, J. Rhoads and R. Baskaran, Parametrically excited MEMS-based filters, *The IUTAM Symposium on Chaotic Dynamics and Control of Systems and Processes*, Rome, Italy (2003), 8–13.
[7] J.F. Rhoads, S.W. Shaw and K.L. Turner, The nonlinear response of resonant microbeam systems with purely-parametric electrostatic actuation, *IEEE Journal of Micromechanics and Microengineering* **16** (2006), 890–899.
[8] A. Vyas, A.K. Bajaj, A. Raman and D. Peroulis, Nonlinear micromechanical filters based on internal resonance phenomenon, in: *Topical Meeting on Silicon Monolithic Integrated Circuits in RF Systems (SiRF'06)*, Digest of Papers, San Diego, CA (2006), 35–38.
[9] B.K. Hammad, E.M. Abdel-Rahman and A.H. Nayfeh, Modeling and analysis of electrostatic MEMS filters, *Nonlinear Dynamics* **60** (2010), 385–401.
[10] B.K. Hammad, A.H. Nayfeh and E.M. Abdel-Rahman, A study of subharmonic excitation of mechanically coupled microbeams for filtration, in: *Proc ASME Int Mechanical Engineering Congress and Exposition*, Boston, Massachusetts, IMECE2008–66728 (2008).
[11] D.S. Greywall and P.A. Busch, Coupled micromechanical drumhead resonators with practical application as electromechanical bandpass filters, *Journal of Micromechanics and Microengineering* **12**(6) (2002), 925–938.
[12] M.T.A. Saif, On a tunable bistable MEMS – theory and experiment, *J Microelectromech Syst* **9** (2000), 157–170.
[13] N.D. Masters and L.L.A. Howell, Self-retracting fully compliant bistable micromechanism, *J Microelectromech Syst* **12** (2003), 73–80.
[14] I.H. Hwang, Y.S. Shim and J.H. Lee, Modeling and experimental characterization of the chevron-type bi-stable microactuator, *J Micromech Microeng* **13** (2003), 48–54.
[15] J. Qui, J.H. Lang and A.H.A. Slocum, Curved beam bistable mechanism, *J Microelectromech Syst* **13** (2004), 137–146.
[16] J. Qui, J.H. Lang, A.H. Slocum and A.C. Weber, A bulk-micromachined bistable relay with U-shaped thermal actuators, *J Microelectromech Syst* **14** (2005), 99–109.
[17] R.A.M. Receveur, C.R. Marxer, R. Woering, V.C.M.H. Larik and N.F. de Rooij, Laterally moving bistable MEMS DC switch for biomedical applications, *J Microelectromech Syst* **14** (2005), 89–98.
[18] S. Krylov, B.R. Ilic, D. Schreiber, S. Seretensky and H. Craighead, The pull-in behavior of electrostatically actuated bistable microstructures, *J Micromech Microeng* **18** (2008), doi: 10.1088/0960-1317/18/5/055026.
[19] K. Das and R.C. Batra, Pull-in and snap-through instabilities in transient deformations of microelectromechanical systems, *J Micromech Microeng* **19** (2009), doi:10.1088/0960-1317/19/3/035008.
[20] A.H. Nayfeh, Nonlinear interactions, Wiley Interscience, New York, 2000.
[21] M. Amabili, Nonlinear vibrations and stability of shells and plates, Cambridge University Press, 2008.
[22] W.Y. Poon, C.F. Ng and Y.Y. Lee, Dynamic stability of a curved beam under sinusoidal loading, *Proceedings of the I MECH E-Part G, J Aero Eng* **216**(4) (2002), 209–217.
[23] S. Krylov and R. Maimon, Pull-in dynamics of an elastic beam actuated by continuously distributed electrostatic force, *J Vib Acoust* **126** (2004), 332–342.
[24] D. Elata and H. Bamberger, On the dynamic pull-in of electrostatic actuators with multiple degrees of freedom and multiple voltage sources, *J Microelectromech Syst* **15** (2006), 131–140.
[25] F.M. Alsaleem, M.I. Younis and H.M. Ouakad, On the nonlinear resonances and dynamic pull-in of electrostatically actuated resonators, *J Micromech Microeng* **19** (2009), 45–58.
[26] J. Humphreys, On dynamic snap buckling of shallow arches, *AIAA J 4* **5** (1966), 878–886.
[27] M.I. Younis, E.M. Abdel-Rahman and A.H. Nayfeh, A reduced-order model for electrically actuated microbeam-based MEMS, *J Microelectromech Syst* **12** (2003), 672–680.

[28] H.M. Ouakad and M.I. Younis, Nonlinear dynamics of electrically actuated carbon nanotube resonators, *ASME Journal of Computational and Nonlinear Dynamics* **5**(1) (2010), 011009.1–011009.13.
[29] H.M. Ouakad and M.I. Younis, The dynamic behavior of MEMS arch resonators actuated electrically, *Int J Nonlin Mechanics* **45** (2010), 704–713.
[30] V.M. Varadan, K.J. Vinoy and K.A. Jose, RF MEMS and their applications, New York, Wiley, 2003.